IET Electric Power Applications

Research Article

IET Journals
The Institution of Engineering and Technology

Performance investigation of simplified PWM MPPT approach for direct PV-fed switched reluctance motor in water pumping system

ISSN 1751-8660
Received on 19th January 2017
Revised 14th June 2017
Accepted on 17th July 2017
doi: 10.1049/iet-epa.2017.0038
www.ietdl.org

Vijay Babu Koreboina[1] ✉, *B. L. Narasimharaju*[1], *D. M. Vinod Kumar*[1]

[1]*Department of Electrical Engineering, National Institute of Technology, Warangal, Telangana, India*

✉ *E-mail: vbkeed@nitw.ac.in*

Abstract: Variable speed drives (VSDs)-based direct photovoltaic (PV) fed water pumping systems (WPS) are of increasing importance for the socio-economic growth in remote areas. Due to the absence of windings and magnets on the rotor, switched reluctance motor (SRM) is emerging as a viable economic alternative in VSD systems. Thus, this study proposes and presents a simplified pulse width modulation-based maximum power point tracking (MPPT) control for direct PV-fed SRM-WPS using modified lookup table (MLUT) approach. The proposed control technique offers lesser phase peak, near same phase rms, reduced torque ripple and noise, better efficiency and reduced DC-link current ripple in contrast to single pulse mode technique. In addition, the proposed system does not require an intermediate converter and current sensors. Thus, results in reduced noise, reduced size and hence the cost of WPS. Further, it also provides a reduced memory size due to MLUT and an effective MPPT with the good dynamic response for a change in atmospheric conditions. The proposed system is modelled and simulated in MATLAB/Simulink environment and the prototype is built to validate experimentally using field programmable gate array controller. The performance analysis of the proposed system has been carried out and presented.

1 Introduction

With the reduction in the cost of solar cell technology, the demand for standalone direct photovoltaic (PV) fed water pumping systems (WPS) in remote and rural areas is increased. In a developing country like India, where the majority of the population of about 70% is dependent on agriculture as their primary occupation, the standalone PV-fed WPS plays a dominant role in the socio-economic growth. In this context, various reforms for PV-fed WPS were initiated by developing countries like India for the development of remote and rural sectors [1, 2]. One of the key elements in PV-fed WPS is the variable speed drive (VSD) system, presently conventional electrical motors (induction motors, synchronous motors, permanent magnet synchronous motors and permanent magnet DC motors) are mostly used. Switched reluctance motor (SRM) without the windings and magnets on the rotor is emerging as a viable cost-effective alternative to the conventional drives in PV-fed WPS [3, 4].

Further, the SRM is gaining importance in VSD system due to its advantages such as high torque to weight ratio, low cost, high-power density, simple construction, thermal robustness, wide speed range and better efficiency. Extensive research over three decades on SRM and its control has confined its suitability in a wide range of applications such as rail air conditioner, aerospace, electric vehicles, washers. State of the art on SRM for off-grid rural applications such as PV-based WPS, wind and hybrid PV-wind energy systems are reported [5]. In [6], comparative study of PV powered VSD (induction motor, brushless DC motor and SRM) systems are presented. The advantage of lower environmental effect and longer life cycle of SRM in comparison with induction motor drives is presented [4]. A few authors have also addressed the suitability and application of SRM-based PV-fed WPS [7–14]. Table 1 provides an overview of state of the art on PV-fed SRM-WPS application. Many of the control schemes proposed for PV-fed SRM-WPS generally requires sensors, intermediate DC–DC converter stage and power conditioning units. Furthermore, the lack of maximum power point tracking (MPPT)-assisted SRM control, performance characterisation with changing atmospheric conditions, the effect of DC-link current ripple and experimental validation etc. Therefore, PV-fed SRM-WPS motivates a wide scope of research with suitable control to accomplish the following features:

a) Simplified control approach.
b) Cost and size reduction without the requirement of current sensors and intermediate power stages.
c) Better performance indices such as phase peak current, phase rms current, torque ripple, noise, efficiency and DC-link current ripple for SRM.
d) Acclimatise MPPT with the effect of pump load for varying atmospheric conditions.
e) Experimental validation of the theoretical concept.

This paper proposes and presents the performance analysis of pulse width modulation (PWM)-based MPPT control of direct PV-fed SRM-WPS for changing atmospheric conditions. Besides, a modified lookup table (MLUT) with reduced memory size is developed to implement the PWM-based MPPT control. Performance indices of proposed control scheme such as per phase peak and rms current, torque ripple, noise, efficiency and DC-link current ripple are evaluated and compared with the single pulse mode (SPM). An 8/6 3000 rpm SRM coupled with a fan load is used for prototype validation of control techniques using field programmable gate array (FPGA) Spartan 3AN Board. This paper is organised as follows: the introduction in Section 1, Section 2 presents the performance significance of various control schemes for PV-fed WPS. MATLAB/Simulink modeling of SRM and its characterisation using both experimental and simulation approach is discussed in Section 3. Section 4 describes the prototype development and performance investigation of the proposed system. Finally, Section 5 presents conclusions of the proposed work.

2 Direct PV-fed SRM-WPS using PWM MPPT control

Conventional control of SRM consists of operating with hysteresis control mode (HCM) under low-speed operation and with SPM in high-speed operation. The HCM control was evolved due to higher DC-link voltage and low back emf in low-speed range which results in higher phase peak currents. In HCM scheme, the reference current value needs to be maintained within the band limit to meet the required torque levels. However, HCM control needs additional components such as frequency limiters, current

feedback sensors and limiters which increase the control complexity and hence cost. Use of HCM control for direct PV powered SRM-WPS is presented in [7, 8], where the required torque level is maintained by controlling the phase currents at the reference levels as shown by block diagram in Fig. 1*a*.

Authors in [15] have proposed a variable DC (VDC) SPM control, in which the band limiter and its current feedback sensors are not required, since regulating voltage is proportionally comparable to back emf and speed. VDC control operates in SPM mode throughout the speed range, in which current is maintained within the operating range by varying turn-on and turn-off angles [15]. Speed dependent variable DC-link voltage-based SPM control in PV-fed WPS is presented in [9], where the variable DC-link voltage is regulated from PV source by an intermediate DC–DC converter for MPPT tracking as shown in Fig. 1*b*.

Like in VDC SPM control technique, PWM technique also does not require current sensors because of varied duty ratio control with constant switching frequency to maintain the required current levels. However, to achieve VDC an additional intermediate converter is required that leads to increased size and the cost of the system. Therefore, in this work, a direct PV-fed SRM-WPS is proposed, in which an intermediate converter is not required as depicted in Fig. 1*c*. In addition, proposed system using VDC PWM control eliminates the need for current sensors and also provides reduced or zero voltage commutation that results in reduced noise levels. Furthermore, the proposed system uses a new MLUT approach to implement VDC PWM-based MPPT, thus results in reduced memory size when compared with classical two dimensional (2D) lookup table (LUT). The FPGA technology can be used to realise the control techniques since it provides fast realisation of non-linearity in SRM with parallel computational ability when compared with conventional digital signal processors (DSP) [16–19]. Therefore, FPGA technology is used to realise the prototype of the proposed system.

Table 1 Overview of state of the art on PV-fed SRM-WPS application

Authors	SRM objective	Control scheme	Key features
D. Ronanki, 2012 [7]	Torque ripple minimisation	DTC HCM with solar radiation and temperature effect	Reduced DC-link voltage
S. Belliwali, 2012 [8]	Direct-coupled PV SRM pump	HCM with solar radiation effect	Modelling and simulation elimination of converter stage
Hamid M, 1998[9]	Performance analysis of PV pump using SRM	SPM with solar radiation effect	Improvement in matching efficiency
Oshaba, 2015 [10]	PI design for MPPT		Advantages of BAT algorithm compared with PSO
Oshaba, 2015 [11]	PV-fed speed control of SRM		Ant colony optimisation compared with genetic algorithm
Sujitha, 2014 [12]	Standalone PV-fed SRM using repression resistor converter	Conventional low-speed hysteresis and high-speed angle pulse	Energy stored in dump resistor to improve torque production
Oshaba, 2013 [13]	High-speed SRM fed by PV	SPM	Torque and speed control loops for accurate speed control
Dursun, 2008 [14]	Fuzzy logic speed control for PV-fed SRM drive		Intelligent speed control to improve destination distance of wheelchair

3 Modelling and simulation of switched reluctance motor

A simulation model of SRM has been built using LUT-based approach based on the governing (1)–(5) of electrical and mechanical systems. This approach consists of LUT with the current characteristics i (ψ, θ) and the static torque T (i, θ) which are populated by finite element method (FEM) or experimental data. In this work, experimental approach is used to populate the flux-linkage characteristics and to compute static torque characteristics of an 8/6 3000 rpm SRM as given in the Appendix. In this approach, the flux-linkage characteristics are determined by using the rising current method, where a voltage pulse is applied to one of the phases with the rotor being locked at a position using indexing head. The duration of the pulse is maintained until the current is built to a value of about 1.2 times rated current. A digital storage oscilloscope is used to acquire voltage and current to process it further and compute flux-linkage in MATLAB/Simulink. Fig. 2*a* shows the experimental setup for determining flux-linkage characteristics using indexing head to hold the rotor shaft at a position. Fig. 2*b* shows the experimental voltage and current waveforms at the unaligned position of 8/6 SRM. Fig. 2*c* illustrates flux-linkage characteristics which are computed using (2). Due to high reluctance in unaligned position, the flux-linkage characteristics exhibit linearity and at the aligned position characteristics become saturated non-linear due to minimum reluctance. Similarly, the flux-linkage at various positions is obtained, and then the static torque characteristics are developed using co-energy principle. Figs. 2*c* and *d* show the experimentally obtained flux-linkage and static torque characteristics, respectively. Governing equations of SRM are

$$v = i * R + \mathrm{d}\psi/\mathrm{d}t \tag{1}$$

where v is the excitation voltage, i is the phase current, R is the phase resistance, and ψ is the flux linkage. Instantaneous torque can be calculated through following equations using co-energy principle:

$$\psi = \int (v - i * R)\mathrm{d}t \tag{2}$$

$$w' = \int_0^i \psi \, \mathrm{d}i \tag{3}$$

$$T_e = \left.\frac{\partial w'}{\partial \theta}\right|_{i\,=\,\text{constant}} \tag{4}$$

where w' is the co-energy, T_e is the torque and θ is the rotor position. The total torque (T) can be given as

$$T = \sum_{j=1}^{4} T_{ej} = J\frac{\mathrm{d}\omega}{\mathrm{d}t} + B \times \omega + T_{\mathrm{L}} \tag{5}$$

where j is the phase number, ω is the speed, J is the inertia, B is the friction coefficient and T_{L} is the load torque.

4 Implementation and experimental analysis of proposed system

4.1 Performance investigation of direct PV-fed SRM-WPS

Performance parameters such as phase peak current, rms current, torque ripple, noise and efficiency play a major role for SRM to evaluate its suitability in various applications. Hence, these parameters are to be investigated in specific with MPPT of direct PV-fed SRM-WPS. Phase peak current determines the safe operating current conditions especially under low-speed operation where current may reach higher values because of low back emf.

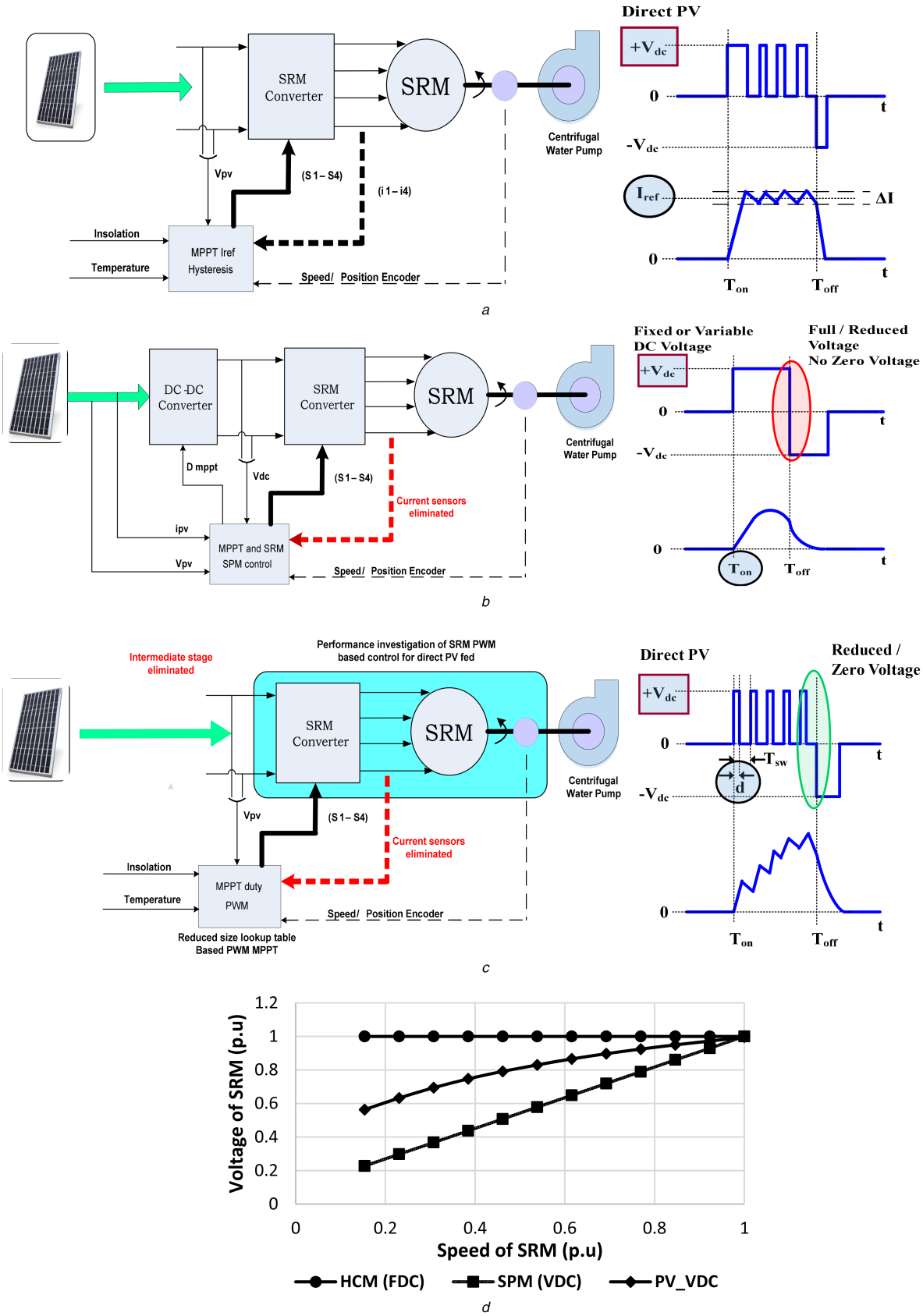

Fig. 1 *Block diagrams*

(a) Block diagram of HCM-based control for PV-fed SRM-WPS [8] without intermediate DC–DC converter, ***(b)*** Block diagram of SPM-based variable voltage control for PV-fed SRM-WPS [9] without current sensors, ***(c)*** Block diagram of proposed PWM-based MPPT control for direct PV-fed SRM-WPS without sensors and DC–DC converter and, ***(d)*** Voltage versus speed curves of proposed system with various control schemes

Phase rms value determines the I^2R loss in the winding which needs to be minimal for better performance. Torque ripple is a measure of noise levels in SRM, hence minimisation of torque ripple results in reduced noise levels. Further, the DC-link current ripple plays a key role in PV powered system. Authors in [20, 21] have been investigated and formulated the effect of the current ripple of PV powered DC–DC converter. However, the effect of current ripple for PV-fed SRM-WPS is yet to be investigated using a suitable controller. Thus, the effect of control scheme on current

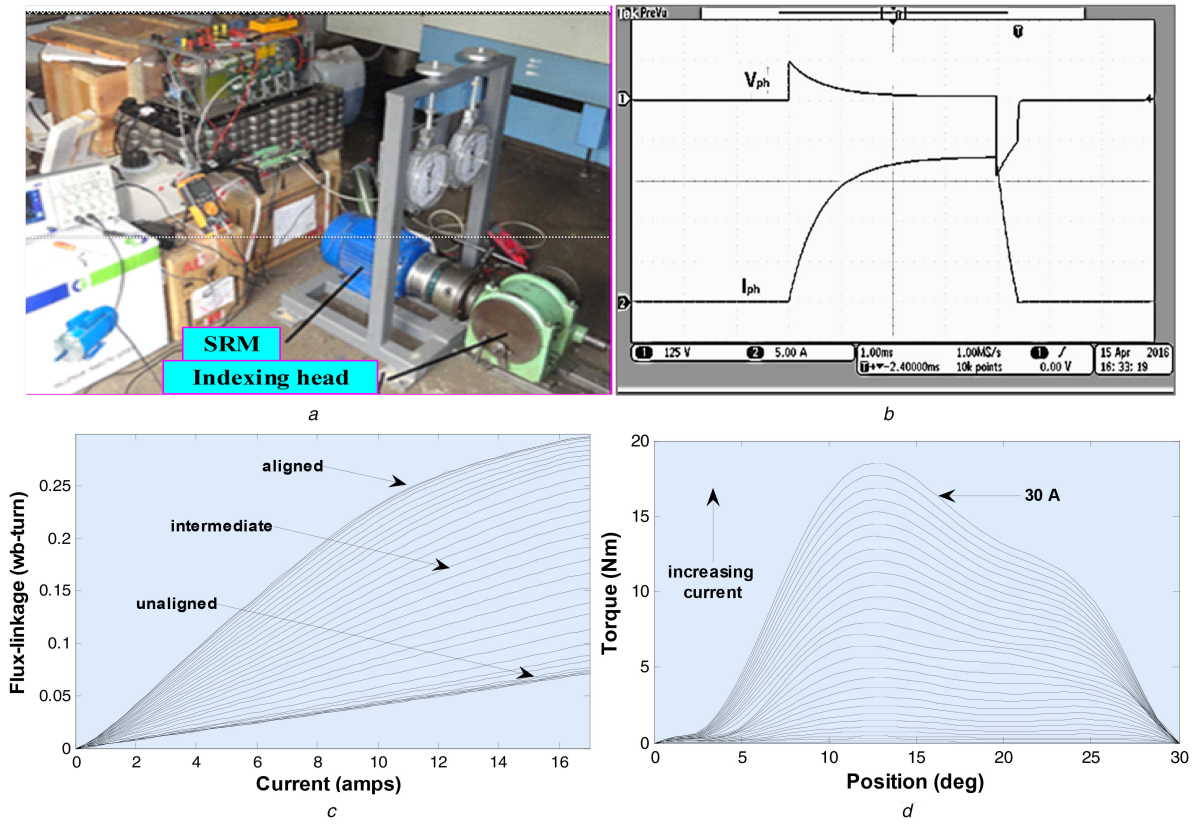

Fig. 2 *Experimentally obtained flux-linkage and static torque characteristics*

(a) Experimental setup to determine flux-linkage characteristics. Voltage and current waveforms to compute flux-linkage at various rotor positions, ***(b)*** Unaligned 0°. Experimental characteristics of SRM, ***(c)*** Flux-linkage curves, ***(d)*** Static torque curves

ripple is also presented as performance indices in PV-fed SRM-WPS.

One of the key features of SRM is its scalability of control schemes to operate in fixed DC bus voltage (FDC) as well as with variable DC bus voltage (VDC). Few authors have presented the control schemes modification to operate in variable DC bus voltage in SPM mode throughout speed range with advantages such as the elimination of hysteresis band and hence current feedback sensors, reduction in noise and also improvise the efficiency. In this work, the performance parameters (phase peak current, phase rms current, torque ripple, noise and efficiency) are investigated to elevate the advantages of operating with variable DC bus voltage in specific with PWM control for SRM feeding quadratic type load. Figs. 3*a* and *b* depict the DC bus voltages for various schemes and quadratic pump load characteristics considered for simulation. Simulations are carried out in MATLAB/Simulink environment. Figs. 3*c* and *d* show the simulated phase resultant torques of FDC SPM, FDC PWM VDC SPM and VDC PWM control schemes with fixed turn-off angle. Tables 2 and 3 present the phase peak and rms currents of all the schemes. From Figs. 3*c* and *d*, Tables 2 and 3, it can be observed that for near same rms, the PWM technique with VDC principle results in reduced torque ripple and peak currents under low speeds when compared with SPM technique.

Fig. 4*a* depicts the prototype experimental setup of an 8/6 3000 rpm SRM machine with fan load (as an emulation of quadratic pump load) for concept validation. Simulation and implementation were carried out to identify best performance combination of turn-on and turn-off angles ((−3.75° and 11.25°), (1.25° and 16.25°) and (6.25° and 21.25°)) for PWM control and in case of SPM T_{off} combinations (11.25, 16.25 and 21.25). Among these for PWM (6.25 and 21.25) and for SPM (16.25) combinations exhibited better performance which are used for further performance investigation. Figs. 4*b* and *c* depict the speed–voltage relationship considered for various control schemes and the fan load power characteristics curve. All the control techniques are developed in FPGA Spartan 3AN board. Altium Designer software is used to build control logic and interface between PC and board. For FPGA implementation, these techniques are modelled and simulated initially in MATLAB/Simulink environment using a Xilinx System Generator and are realised in Xilinx Spartan 3AN nanoboard. Figs. 5*a–d* show the experimentally measured peak current, rms current, noise and efficiency characteristics as a function of speed for all the above control schemes. From these characteristics, it can be observed that the VDC PWM technique provides better performance in SRM-WPS like; reduced peak current, near same rms, lesser torque ripple, and lower noise. In addition, improved efficiency due to reduced device and core losses in case of VDC PWM technique as compared FDC counterparts. Although, the variable DC concept offers wide advantages, but the presence of front-end DC–DC converter for achieving variable DC leads to various demerits such as additional power stage and its control circuit, increased size and hence higher cost. In contrast, proposed direct PV-fed variable voltage system does not require front-end DC–DC converter. Thus, assures low cost, compact size and improved performance. Therefore, this paper proposes a direct PV-fed SRM-WPS using PWM-based MPPT control for which performance indices need to be investigated when compared with SPM control counterpart. The performance parameters of the controller are to be investigated at various steady-state peak power points predetermined at different operating insolation and temperature conditions.

For concept validation of direct PV-fed SRM-WPS, prototype experimental setup consists of a programmable DC source configured as PV source to power the SRM coupled fan load (as an emulation of WPS) is illustrated as shown in Fig. 4*a*. The PV array used in this study consists of as string with 261 cells in series to meet fan load, such that the overall terminal voltage (v_{array}) and PV power (P_{array}) at ambient temperature [22] is given by

$$v_{\text{array}} = 20.3841 \times \log_{\text{e}}\left(\frac{I_{\text{ph}} - I_{\text{array}} + I_{\text{s}}}{I_{\text{s}}}\right) - 13.05 \times I_{\text{array}} \quad (6)$$

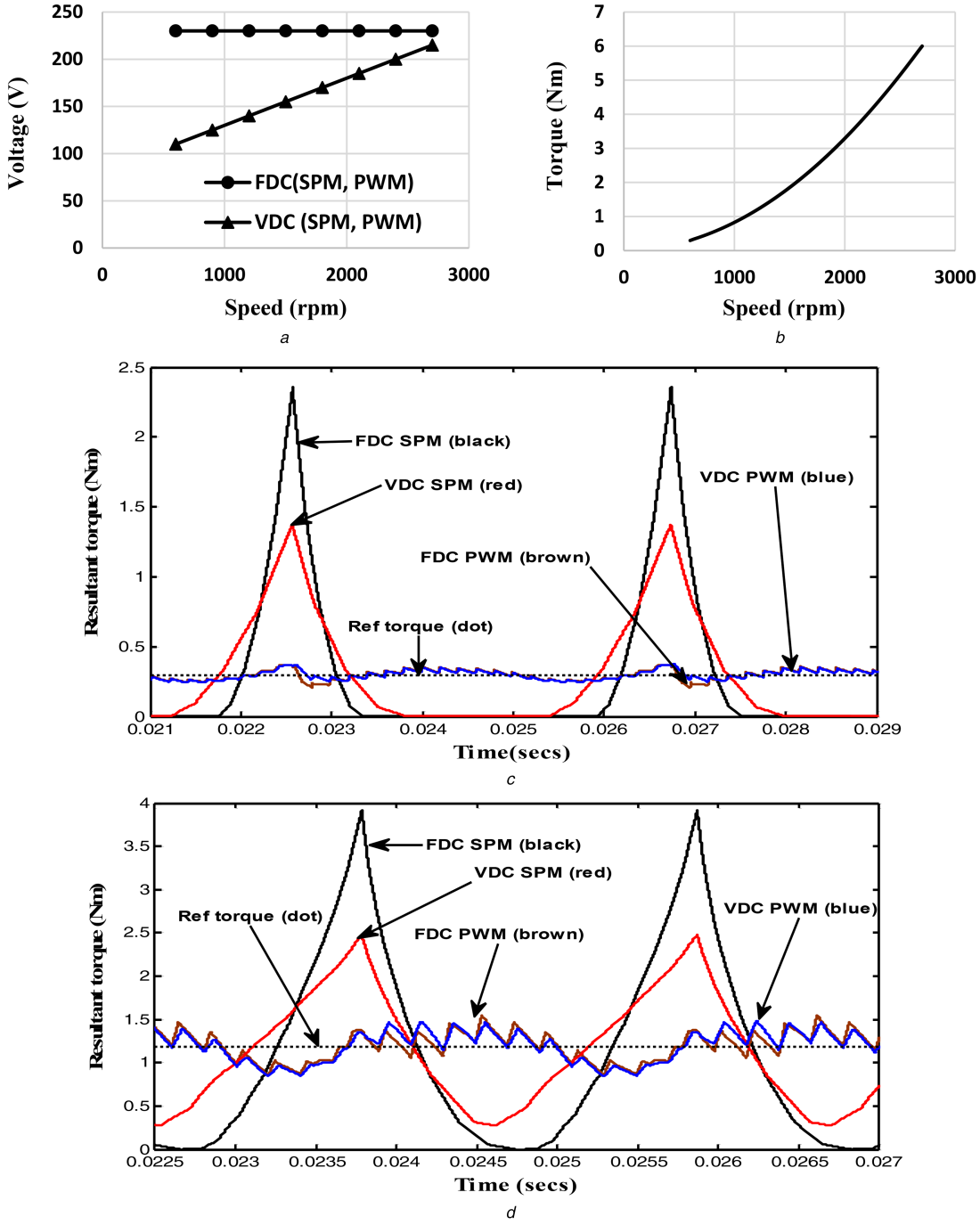

Fig. 3 *DC bus voltages*

(a) Fixed and variable DC voltages for the various control schemes, ***(b)*** Quadratic load speed-torque profile. Resultant torque of all four control schemes (FDC SPM, FDC PWM, VDC SPM and VDC PWM) at ***(c)*** 600 rpm, 0.296 Nm, ***(d)*** 1200 rpm, 1.185 Nm

Table 2 Phase peak current (in Amps) at different speeds for control schemes

Speed, rpm	FDC SPM	FDC PWM	VDC SPM	VDC PWM
600	10.17	3.97	7.84	3.92
900	11.73	6.01	9.23	5.85
1200	13.04	8.05	10.41	7.80
1500	14.05	9.90	11.41	9.56
1800	14.81	11.35	12.35	10.80
2100	15.39	13.07	13.30	12.55
2400	15.80	13.87	14.31	13.37
2700	16.20	14.82	15.42	14.83

$$p_{\text{array}} = I_{\text{array}} \times 20.3841 \times \log_{\text{e}}\left(\frac{I_{\text{ph}} - I_{\text{array}} + I_{\text{s}}}{I_{\text{s}}}\right) - 13.05 \times (I_{\text{array}})^2 \quad (7)$$

where I_{array} is the array current, I_{ph} is the insolation and temperature dependent photocurrent, I_{s} is the temperature dependent diode current, T_{c} is the cell temperature, k is the Boltzmann constant (1.38×10^{-23} J/K), 'A' is diode ideal factor, R_{s} is the series cell resistance and 'q' is the electron charge (1.6×10^{-19} C). The equation model of I_{ph} and I_{s} are considered as follows:

$$I_{\text{ph}} = (I_{\text{sc}} + k_i \times (T_{\text{c}} - T_{\text{ref}})) \times G \quad (8)$$

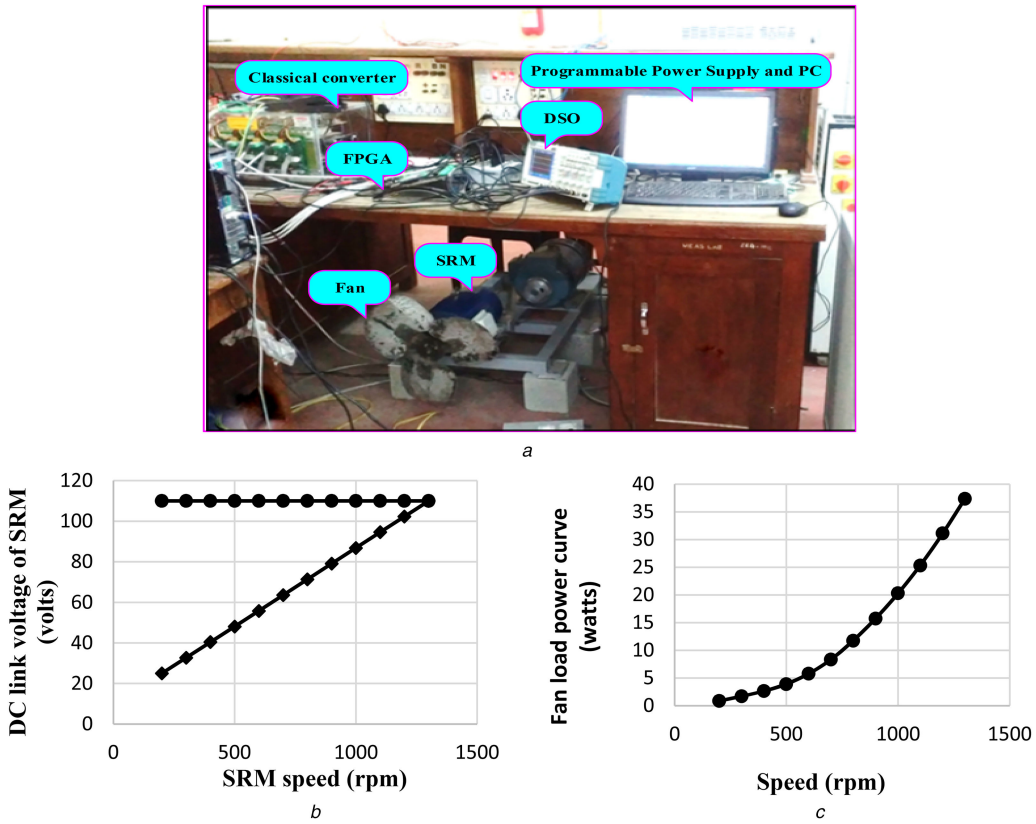

Fig. 4 *Prototype experimental*

(a) Prototype experimental setup SRM with fan load, ***(b)*** Voltage–speed characteristics of fixed (filled circle) and variable DC (filled diamond) fed SRM, ***(c)*** Fan load power curve

$$I_s = I_{rs} \times \left(\frac{T_c}{T_{ref}}\right)^3 \times \exp\left(\frac{qE_g}{kA}\left(\frac{1}{T_{ref}} - \frac{1}{T_c}\right)\right) \quad (9)$$

where I_{sc} is the cell short-circuit current at 25°C and the standard value of a solar insolation (1 kW/m^2), k_i is the temperature coefficient of cell current (A/°C), T_{ref} is the cell reference temperature and G is a solar insolation (kW/m^2), I_{rs} is the cell reverse saturation current at the reference temperature and the solar radiation, and E_g is the bang-gap energy of the semiconductor used in the cell.

Figs. 6*a* and *b* depict the PV current, power and maximum power characteristics versus voltage for various insolation and temperature levels.

Initially, the system is operated with the pre-calculated maximum voltage at steady-state maximum power point for various atmospheric conditions and the control parameters are varied to achieve maximum current. The performance parameters at these steady-state operating conditions are then measured experimentally for SPM and PWM control techniques. Figs. 7*a–d* show the experimental phase voltage and current SPM and PWM control strategies, respectively, at insolation levels (G) of 0.6 and 0.9 kW/m^2 with temperature (T) of 25°C. From these experimental results, the characteristics curves of peak and noise are plotted as shown in Figs. 8*a* and *b* for various values of G. It can be observed from Figs. 8*a* and *b* that the PWM technique offers less peak and lower noise levels (measured with sound level meter at ambient as 57 dB). Figs. 9*a* and *b* show the DC-link current waveforms which indicate the significance of ripple current for SPM and PWM control schemes, respectively, at 0.5 kW/m^2. From Figs. 9*a* and *b*, it confirms that the PWM offers a reduced ripple current when compared with SPM control counterpart. As a consequence of less current ripple in DC link can ensure an effective MPPT with less oscillation. Furthermore, Table 4 describes the performance comparisons of various control techniques at $G = 0.5$ kW/m^2. It can be noticed from Table 4 that the PWM technique offers better efficiency without the necessity of current sensors.

Table 3 Phase rms current (in Amps) at different speeds for control schemes

Speed, rpm	FDC SPM	FDC PWM	VDC SPM	VDC PWM
600	1.827	1.846	1.835	1.846
900	2.703	2.786	2.695	2.776
1200	3.568	3.702	3.542	3.701
1500	4.409	4.607	4.372	4.604
1800	5.243	5.503	5.238	5.491
2100	6.105	6.397	6.143	6.401
2400	7.079	7.314	7.185	7.351
2700	8.211	8.315	8.303	8.35

These comparative assertions confirm that the PWM technique for direct PV-fed SRM-WPS offers reduced peak current, torque ripple, noise levels, current ripple, and better efficiency over SPM [9] counterpart. HCM-based direct PV-fed WPS [7] eliminates the need for intermediate converter stage, whereas in SPM-based PV-fed WPS [9] eliminates the need for sensors but it requires an intermediate converter. The proposed PWM technique for direct PV-fed WPS does not require both the intermediate converter [7] and sensors [9] and hence, provide improved performance with less cost.

4.2 MLUT-based PWM MPPT control of direct PV-fed SRM-WPS

Various MPPT techniques are reported in the literature such as P&O, incremental conductance, fractional open-circuit voltage, fuzzy logic control, artificial neural network (ANN), pre-computed LUT approach which can be classified into search methods or knowledge-based methods. Each is having their own merits and demerits based on their application, cost and sensor requirements etc. Among knowledge-based methods which usually developed based on PV array information, the LUT-based and ANN approach is the most widely used schemes. The LUT approach is simpler with interpolation and extrapolation but it requires high memory size. ANN approach has the ability to process the knowledge under varying conditions but it requires high computational time in

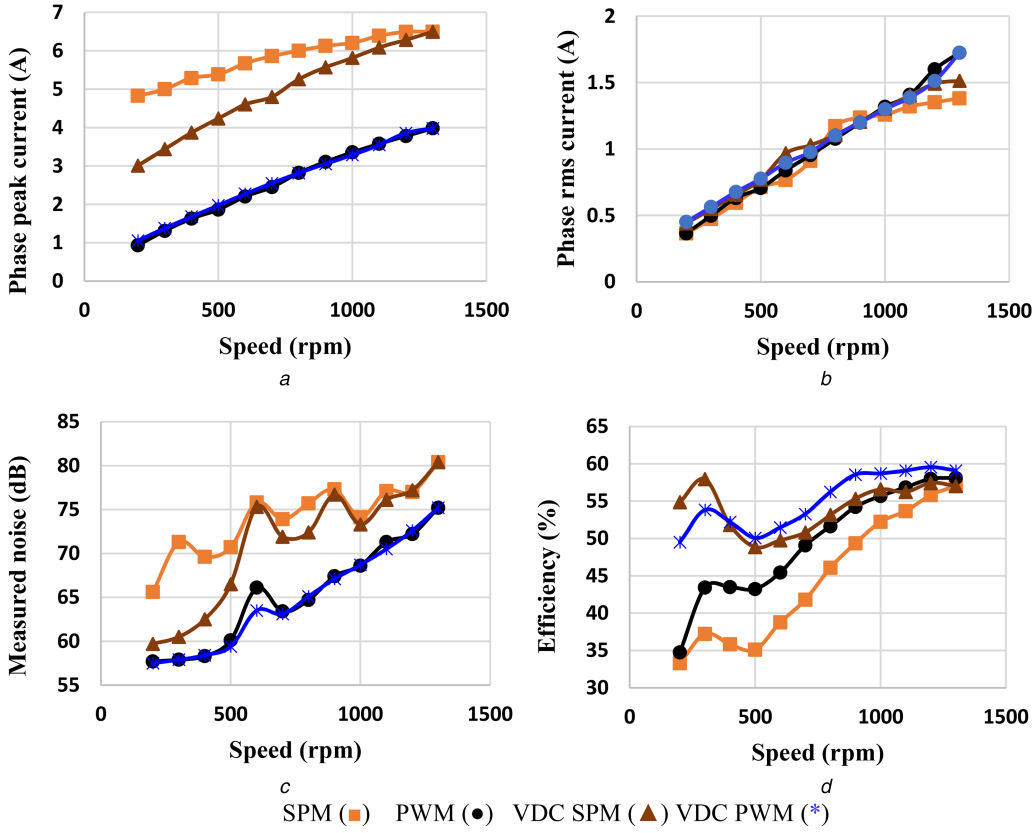

Fig. 5 *Characteristics of various performance parameters versus speed for all control schemes*
(a) Peak current, ***(b)*** Phase rms current, ***(c)*** Noise (at ambient 57), ***(d)*** Efficiency

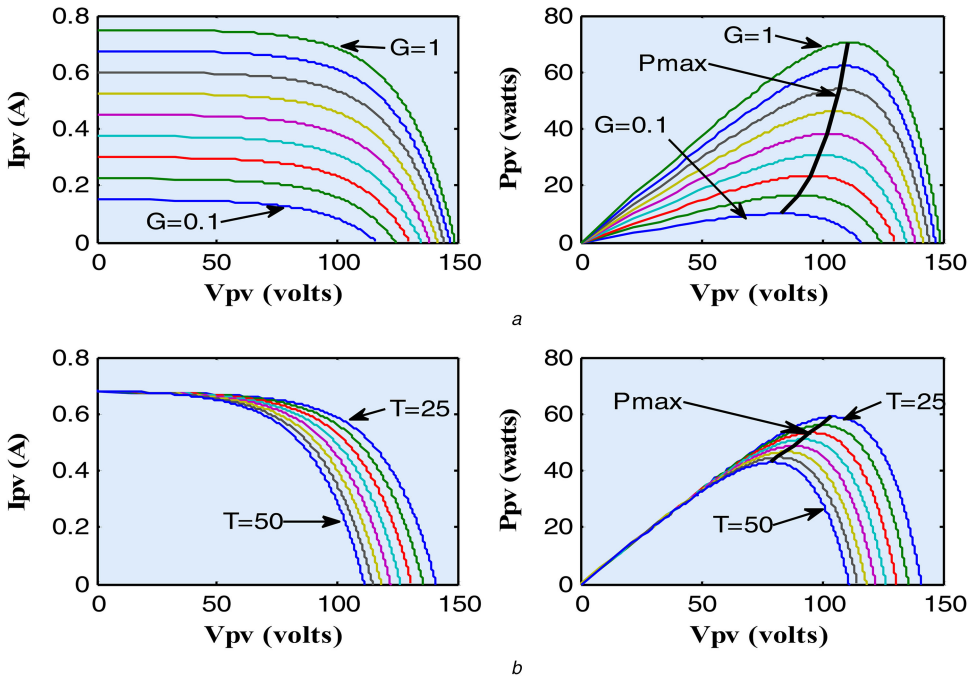

Fig. 6 *PV array characteristics curves*
(a) For various G values (0.1 : 0.1 : 1 kW/m^2) at $T = 25$°C, ***(b)*** For various T values (25 : 2.5 : 50°C) at $G = 1$ kW/m^2

comparison with LUT approach. To evident merits and demerits, LUT and ANN approaches are tested in real-time dSPACE 1104 controller and it is found that the execution time for LUT approaches is 2.84 µs and for ANN approach is 13.55 µs. Although, the LUT approach takes less computational time and provides a faster response but it needs high memory size. In addition, the direct realisation of 2D LUT in FPGA is not possible since it requires concatenation of any two inputs to create an address field for storing the output data. Thus in contrast to LUT conventional 2D LUT, the MLUT with two single (1D) LUT's using polynomial approach is implemented as depicted in Fig 10*a* that aid in reducing the memory size requirement. It can be observed from Fig 10*a* that the 2D LUT has 9 × 6 data (9 insolation points and 6 temperatures points) is modified into two 9 × 1 1D LUT. Matlab instructions such as 'zeros' and 'whos' are used to understand the significance of MLUT. For example, the data points were pre-interpolated and extended with 2D LUT of size 100 × 25 (100 insolation points and 25 temperatures points) whose memory

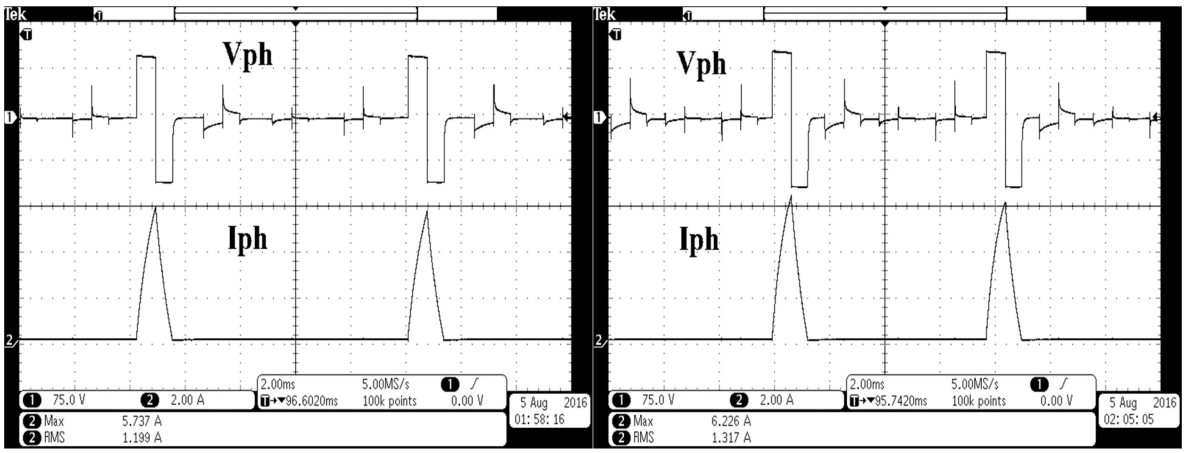

Fig. 7 *Experimentally measured phase voltage and current*
(a) SPM control at ($G = 0.6$ and 0.9 kW/m^2, $T = 25°C$, $T_{off} = 15°$), ***(b)*** PWM control at ($G = 0.6$ and 0.9 kW/m^2, $T = 25°C$, $T_{on} = 6.25°$, $T_{off} = 21.25°$)

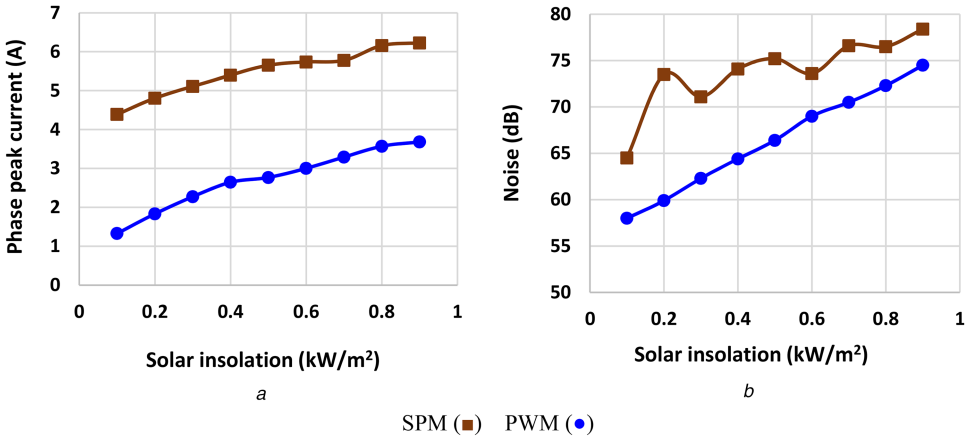

Fig. 8 *Performance characteristics of direct PV-fed SRM-WPS*
(a) Peak current, ***(b)*** Noise (at ambient 57)

size is 20,000 bytes. The MLUT with two 1D LUT (100×1) requires a memory size of 1600 bytes (800 bytes each) which is significantly less when compared with LUT with a memory size of 20,000 bytes.

Thus, this paper proposes a PWM-based MPPT using MLUT approach for direct PV-fed SRM-WPS. The required LUT data is extracted through an experimentation where the duty cycle is varied manually to achieve maximum power point on *I–V* curves for various insolation and temperature levels. Using experimental data, the MLUT is developed and realised in Matlab/Simulink as depicted in Fig 10*b* to test its estimation of PWM duty. Table 5 shows the comparison of MLUT estimated data with that of 2D LUT data for two different temperatures. From Table 5, it is clearly evident that the MLUT results in reduced memory size significantly while retaining near same execution time and estimated duty at far with 2D LUT approach. Fig. 11*a* illustrates the flow chart for development of MLUT (on the left side) and its real-time control in FPGA for changing atmospheric conditions as depicted (on the right side). The solar PV-based variable voltage source is emulated and realised using a dSPACE-controlled

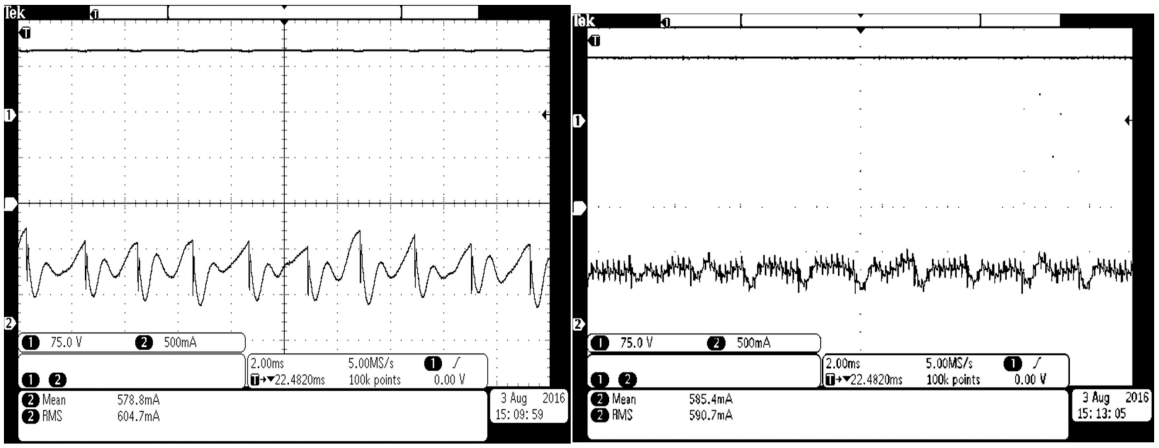

a *b*

Fig. 9 *DC-link current with ripple (scaling factor of 0.54)*
(a) SPM control, ***(b)*** PWM at 0.5 kW/m^2 and 25°C

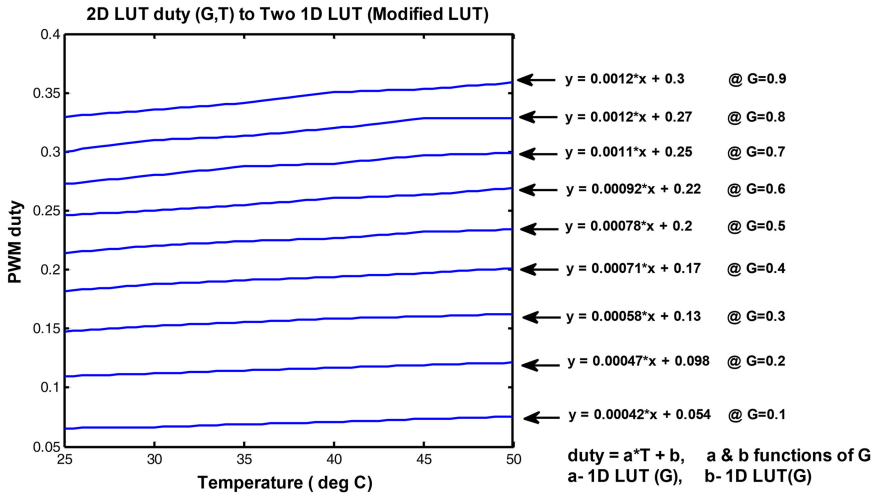

a

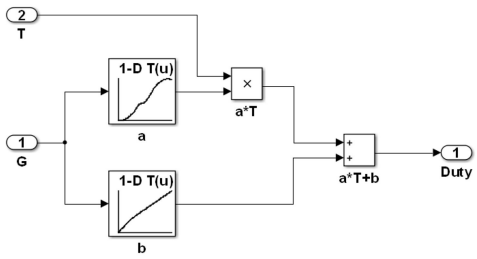

b

Fig. 10 *LUT's using polynomial approach*
(a) Converting 2D LUT into two 1D LUT using MLUT, ***(b)*** Its realisation in Matlab/Simulink

programmable DC power supply. Based on emulated PV source VDC PWM using MLUT approach for SRM control is realised using FPGA Spartan 3AN board. Then, the proposed PV-fed SRM-WPS is validated and tested at various temperature and insolation levels. Figs. 11*b* and *c* depict the simulated and experimental SRM speed response with dynamical change in insolation and temperature. Fig. 12 illustrates the experimental MPPT (P_{max}) curves of PV array for various insolation levels at a temperature of 25 and 50°C, respectively. The results show the conceptual validity and effectiveness of the proposed PWM MPPT with MLUT for changing atmospheric test conditions. From Tables 6 and 7, it can be observed that VDC PWM technique exhibits simple duty control, lower noise and better performance of proposed direct PV-fed WPS.

Table 4 Comparisons of various control techniques at G = 0.5 kW/m^2

Control	SPM	PWM
V_{dc}, V	99.062	99.062
I_{dc}, A	0.31	0.31
output speed, rpm	908	936
output power, W	15.944	17.1711
efficiency	51.75	55.91
sensors	no	no

5 Conclusions

This work proposes and presents the performance of direct PV-fed SRM-WPS using PWM-based MPPT control with MLUT. The proposed system is modelled in MATLAB/Simulink environment using experimentally determined flux-linkage characteristics. The PWM-based MPPT control with MLUT is realised using FPGA

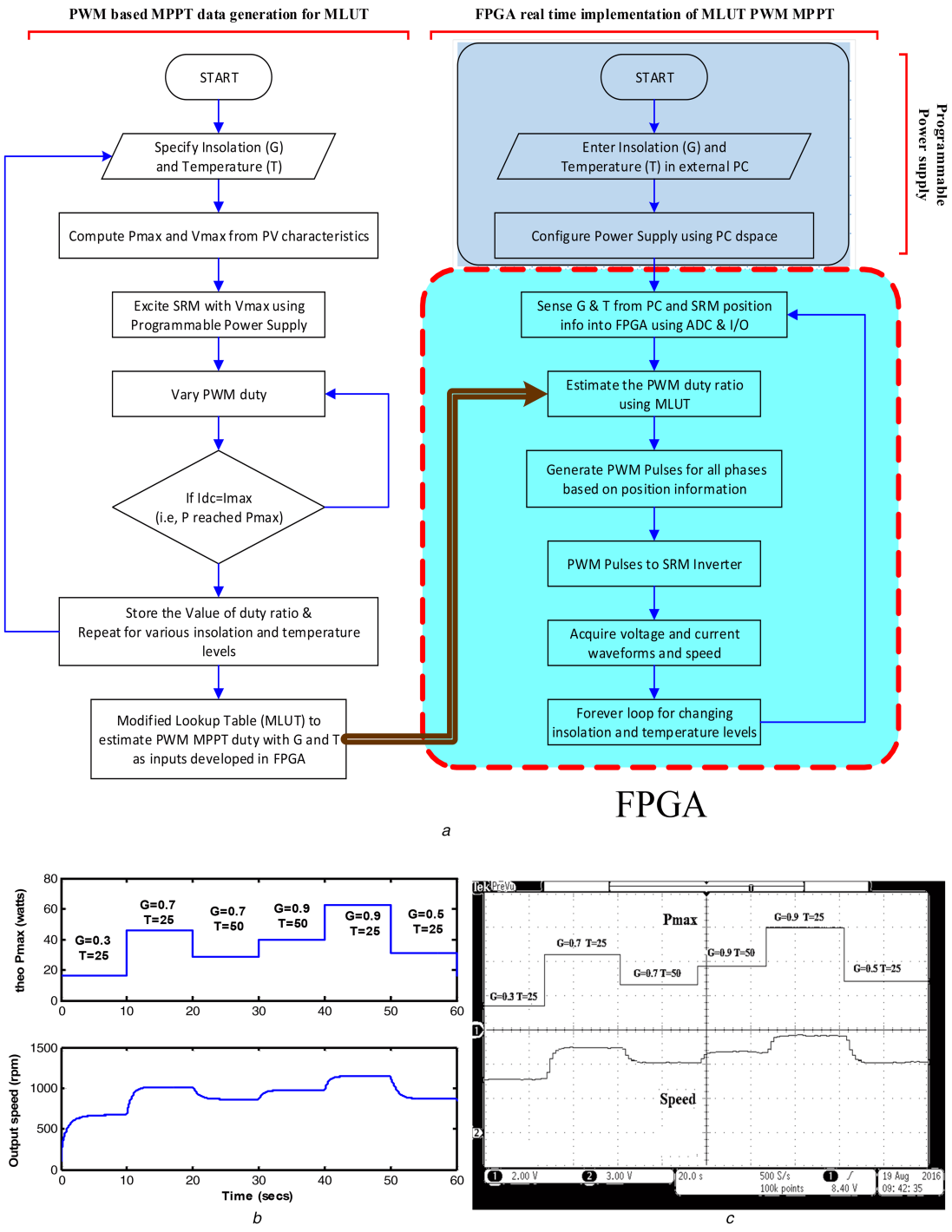

Fig. 11 *Flow chart for development of MLUT*

(a) Modified lookup table-based PWM MPPT data generation and implementation flow chart, ***(b, c)*** Simulated and experimental SRM speed (10 V/1500 rpm) at P_{max} (10 V/100 W) for various insolation and temperature levels

controller for experimental validation of the proposed system. The prototype of proposed WPS has been built and tested using fan load. Experimental result analysis is found to be in close consent with the simulation counterparts. Performance indices such as phase peak and rms current, torque ripple, noise, efficiency and DC-link current ripple of PV-fed WPS using PWM and SPM techniques are compared and analysed for SRM-WPS at various operating insolation and temperature levels. It is evident from these performance comparisons that the proposed PWM technique resulting in the following advantages:

- Simplified control scheme.
- No requirement of current sensors and limiters.
- Elimination of intermediate DC–DC converter thus simplifies control scheme and facilitates the direct PV-fed VDSs.
- Offers lesser peak, near same rms, reduced torque ripple and noise, better efficiency and reduced DC-link current ripple in comparison to SPM mode.
- Reduced computational memory size for duty ratio estimation.
- Effective MPPT for dynamical changes in insolation and temperature conditions.

Aforesaid assertions reveal that the PWM MPPT with MLUT is a viable simplified control scheme in direct PV-fed SRM-WPS.

6 Acknowledgment

The authors thank MHRD, India, and Director, National Institute of Technology Warangal for providing necessary facilities.

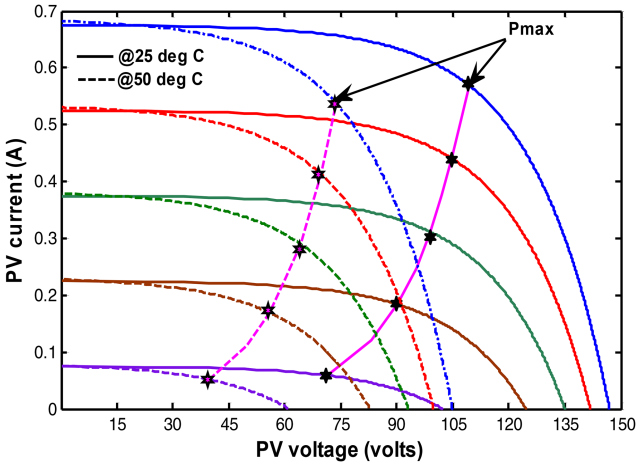

Fig. 12 *Experimental MPPT (P_{max}) curves of PV array for various insolation levels at 25 and 50°C*

Table 5 Comparison of 2D LUT and proposed MLUT

G, kW/m^2	LUT 2-DMemory: 20,000 bytes, execution time = 2.84 µs		MLUTMemory: 1600 bytes, execution time = 2.88 µs	
	Duty at T = 25°C	Duty at T = 50°C	Duty at T = 25°C	Duty@ T = 50°C
0.1	0.0655	0.0754	0.0654	0.0756
0.2	0.1097	0.1212	0.1104	0.1222
0.3	0.1475	0.1624	0.1505	0.1650
0.4	0.1820	0.2014	0.1807	0.1989
0.5	0.2143	0.2340	0.2107	0.2302
0.6	0.2460	0.2692	0.2409	0.2639
0.7	0.2726	0.2990	0.2711	0.2986
0.8	0.3002	0.3288	0.3012	0.3312
0.9	0.3298	0.3585	0.3312	0.3625

Table 6 Overview comparison of the control strategies of SRM-WPS over wide operating speeds

Performance/ control	Peak current	Zero voltage commutation	Torque ripple and noise	Efficiency	DC-link current ripple
FDC SPM	high	no	high	poor	high
FDC PWM	low	yes	low	poor	low
VDC SPM	high	no	high	better	high
VDC PWM	low	yes	low	better	low

Table 7 Overview comparison of the control strategies realisation of PV-fed SRM-WPS

Performance/ control	Intermediate converter	Current sensors and conditioning units	Control parameter
FDC SPM	yes	no	T_{on}
FDC HCM	yes	yes	I_{ref}
FDC PWM	yes	no	duty
VDC SPM	yes	no	T_{on}
VDC PWM	yes	no	duty
direct PV SPM	no	no	T_{on}
direct PV HCM	no	yes	I_{ref}
direct PV PWM	no	no	duty

7 References

[1] Singh, D., Sharma, N.K., Sood, Y.R., *et al.*: 'Global status of renewable energy and market: Future prospectus and target'. Proc. Int. Conf. IET Sustainable Energy and Intelligent Systems, Chennai, 2011, pp. 171–176

[2] Kamalapur, G.D., Udaykumar, R.Y.: 'Rural electrification in India and pre-sizing of solar home systems'. IEEE Global Humanitarian Technology Conf. – South Asia Satellite (GHTC-SAS), Trivandrum, 2014, pp. 13–18

[3] McCoy, G.A.: 'Super premium efficiency motors are now available'. Energy efficiency factsheet, Washington State University. Extension energy program, 2010, pp. 1–5

[4] Andrada, P., Blanqué, B., Martínez, E., *et al.*: 'Environmental and life cycle cost analysis of one switched reluctance motor drive and two inverter-fed induction motor drives', *IET Electr. Power Appl.*, 2012, **6**, (7), pp. 390–398

[5] Vijay Babu, K., Narasimharaju, B.L., Vinod Kumar, D.M.: 'Switched reluctance machine for off-grid rural applications: a review', *IETE Tech. Rev.*, 2016, **33**, (4), pp. 428–440

[6] Domijan, A., Buchh, T.A.: 'Photovoltaic array driven adjustable speed heat pump and power system scheme for a lunar based habitat', *IEEE Trans. Energy Convers.*, 1998, **13**, (4), pp. 366–372

[7] Ronanki, D., Parthiban, P.: 'PV-battery powered direct torque controlled switched reluctance motor drive'. Power and Energy Engineering Conf., Shanghai, 2012, pp. 1–4

[8] Belliwali, S., Chakravarti, A., Raju, A.B.: 'Mathematical modelling and simulation of directly coupled PV WPS employing switched reluctance motor', *IEEE PES Innovative Smart Grid Technol., India*, 2011, pp. 386–390

[9] Metwally, H.M.B., Anis, W.R.: 'Performance analysis of PV pumping systems using switched reluctance motor drives', *J. Solar Energy*, 1996, **56**, (2), pp. 161–168

[10] Oshaba, A.S., Ali, E.S., Abd Elazim, S.M.: 'PI controller design for MPPT of photovoltaic system supplying SRM via BAT search algorithm', *Neural Comput. Appl.*, 2015, **2**, pp. 51–60

[11] Oshaba, A.S., Ali, E.S., Abd Elazim, S.M.: 'ACO based speed control of SRM fed by photovoltaic system', *Electric. Power Energy Syst.*, 2015, **67**, pp. 529–536

[12] Sujitha, S., Venkatesh, C.: 'Analysis of regulated PV fed switched reluctance motor drives using repression resistor converter', *Int. J. Eng. Technol.*, 2014, **6**, (3), pp. 1309–1313

[13] Oshaba, A.S.: 'Control strategy for a high speed SRM fed from a photovoltaic source', *Res. J. Appl. Sci. Eng. Technol.*, 2013, **6**, (17), pp. 3174–3180

[14] Dursun, M.: 'A wheelchair driven with fuzzy logic controlled switched reluctance motor supplied by PV arrays', *J. Appl. Sci.*, 2008, **8**, (19), pp. 3351–3360

[15] Koreboina, V.B., Venkatesha, L.: 'Modelling and simulation of switched reluctance generator control for variable speed wind energy conversion systems'. Proc. Int. Conf. IEEE Power Electronics, Drives and Energy Systems Conf., Bangalore, 2012

[16] Lin, F.J., Teng, L.T., Chen, C.Y., *et al.*: 'FPGA-based adaptive back stepping control system using RBFN for linear induction motor drive', *IET Electr. Power Appl.*, 2008, **2**, (6), pp. 325–340

[17] Dufour, C., Cense, S., Belanger, J.: 'FPGA-based switched reluctance motor drive and DC-DC converter models for high-bandwidth HIL real-time simulator'. 15th European Conf. Power Electronics and Applications (EPE), 2013, pp. 1–8

[18] Stumpf, A., Elton, D., Devlin, J., *et al.*: 'Benefits of an FPGA based SRM controller'. IEEE 9th Conf. Industrial Electronics and Applications (ICIEA), 2014, pp. 12–17

[19] Blaabjerg, F., Kjaer, P.C., Rasmussen, P.O., *et al.*: 'Improved digital current control methods in switched reluctance motor drives', *IEEE Power Electron.*, 1999, **14**, (13), pp. 563–572

[20] El Khateb, A.H., Rahim, N.A., Selvaraj, J., *et al.*: 'DC-to-DC Converter with low input current ripple for maximum photovoltaic power extraction', *IEEE Trans. Ind. Electron.*, 2015, **62**, (4), pp. 2246–2256

[21] Darwish, A., Massoud, A., Holliday, D.: 'Generation, performance evaluation and control design of single-phase differential-mode buck–boost current-source inverters', *IET Renew. Power Gener.*, 2016, **16**, (7), pp. 916–927

[22] Nabil, M., Allam, S.M., Rashad, E.M.: 'Modeling and design considerations of a photovoltaic energy source feeding a synchronous reluctance motor suitable for pumping systems', *Ain Shams Eng. J.*, 2012, **3**, (4), pp. 375–382

8 Appendix

SRM specifications: eight stator poles, six rotor poles, 3000 rpm, 230 V, 11 A, 0.65 Ω classical two switches per phase converter.